Available online at www.sciencedirect.com
ScienceDirect
C. R. Mecanique 336 (2008) 863–872
COMPTES RENDUS MECANIQUE
http://france.elsevier.com/direct/CRAS2B/

Three-dimensional incompressible flow in a two-sided non-facing lid-driven cubical cavity

Brahim Ben Beya *, Taieb Lili

Laboratoire de mécanique des fluides, faculté des sciences de Tunis, département de physique, 2092 El Manar 2, Tunis, Tunisia

Received 11 May 2008; accepted after revision 8 October 2008

Available online 11 November 2008

Presented by Sébastien Candel

Abstract

Numerical simulations of the three-dimensional fluid flow in a two-sided non-facing lid-driven cubical cavity are presented. Computations have been carried out for several Reynolds numbers from a low value to 700. At low Reynolds numbers the flow is steady. The three dimensional flow characteristics are analyzed at $Re = 500$. An analysis of the flow evolution shows that, when increasing *Re* beyond a certain critical value the flow becomes unstable and bifurcates. It is observed that the transition to unsteadiness follows the classical scheme of a Hopf bifurcation. The time dependent solution is studied and the critical Reynolds number is localized. ***To cite this article: B. Ben Beya, T. Lili, C. R. Mecanique 336 (2008).***

Résumé

Écoulement tridimensionnel de fluide incompressible dans une cavité cubique doublement entrainée par des faces adjacentes. Nous présentons dans cette Note une étude numérique de l'écoulement tridimensionnel de fluide dans une cavité cubique doublement entrainée par des faces adjacentes. Les calculs ont été menés à plusieurs valeurs du nombre de Reynolds depuis des valeurs faibles jusqu'à 700. A faible nombre de Reynolds l'écoulement est stationnaire. Les caractéristiques de l'écoulement tridimensionnel ont été analysées à un nombre de Reynolds $Re = 500$. L'analyse de l'évolution de l'écoulement montre qu'avec l'augmentation du *Re* au-delà d'une certaine valeur critique l'écoulement devient instable et subit une bifurcation. Il a été observé que la transition vers l'instationnarité s'effectue par une bifurcation de Hopf. Le nombre de Reynolds critique au-delà duquel l'écoulement devient instationnaire est déterminé. ***Pour citer cet article : B. Ben Beya, T. Lili, C. R. Mecanique 336 (2008).***

Keywords: Fluid mechanics; Incompressible flow; 3D lid-driven cavity; Bifurcation

Mots-clés : Mécanique des fluids ; Fluide incompressible ; Cavité entrainée 3D ; Bifurcation

* Corresponding author.
E-mail address: brahim.benbeya@fst.rnu.tn (B. Ben Beya).

1631-0721/$ – see front matter
doi:10.1016/j.crme.2008.10.004

1. Introduction

The lid-driven cavity (LDC) flows of a Newtonian fluid are regularly the object of researches. Similar flows arise in large variety of natural, industrial and biomedical applications [1]. In addition, the LDC flow is one of the most frequently employed numerical benchmark problems for 2D and 3D [2–6] Navier–Stokes solvers. The majority of papers dealing with the numerical solution of the lid-driven cavity problem have been concerned with the two-dimensional problem.

Papers for the two-dimensional problem incorporating more than one lid-driven have also appeared in the recent literature [7,8]. Recently, Wahba [9] has considered the case of a two sided non-facing lid-driven (TSNFL) cavity in which the flow is driven by two non-facing walls and the four-sided lid driven cavity.

However, despite their apparent simple geometry, a lid-driven cavity flow is known to contain high degrees of complexity, revealing 3D flow structure even at a large spanwise aspect ratio. It exhibits almost all phenomena that can possibly occur in incompressible flows, such as complex 3D patterns, instabilities, transition and turbulence. According to the 2D-LDC, Auteri et al. [10] have localized the critical Reynolds number for the first Hopf bifurcation in the interval (8017.6, 8018.8) using a second-order spectral projection method. Bruneau et al. [4] have situated the critical Reynolds number between 8000 and 8050 within less than 1% of error.

The three-dimensional transport phenomena often differ from the two-dimensional cases under the same boundary conditions due to the three-dimensionality effects.

Three-dimensional structures, called Taylor–Gortler (TG) vortices can be found in most of real flows. For example, the instability problem of transient Couette flow in a cylinder is closely related with that of TG vortices [11]. To study flow characteristics during 3D-LDC flow, numerical and experimental studies have been conducted. Koseff and al. [12] performed experiments and observed TG vortices in a plane normal to the main flow.

Very recently, J. Chicheportiche et al. [13] studied instabilities in the 3D-LDC flow with span wise periodic boundary-conditions (to suppress the role of the end walls) at $Re = 1000$. The authors identified by DNS and global linear stability the mechanisms of transition and found a 3D steady TG flow. This means that the rigid end-walls suppress TG vortices in driven cavities with low span length.

Three-dimensional cavity flow with more than one moving wall does not appear in the literature and, certainly, no attention has been paid to the 3D-TSNFL cavity problem.

The purpose of this paper is to extend the 2D-TSNFL cavity flow which were developed in [9] in three dimensions. The top wall is moving to right, while the left vertical wall is moving down with the same constant velocity. All computations will be made on a grid of 64^3 nodes with the help of an accelerator multigrid solver.

The three-dimensional two-sided non-facing lid (3D-TSNFL) flow structure is first analyzed in the steady case. The further evolution of the flow is qualitatively investigated. According to [13], we believe that the bifurcation reported in this study for the 3D-TSNFL with no-slip end walls in the span wise direction cannot leads to TG vortices. This question remains uncertain at the present time and perhaps a fully linear stability analysis is needed to clarify this matter.

2. Physical model and formulation

We consider the three-dimensional two-sided non-facing lid-driven (3D-TSNFL) cubical cavity with sides of length H, as depicted in Fig. 1. The top wall is moving to right, while the left vertical wall is moving down with the same constant velocity. The cavity is filled with a Newtonian fluid with constant viscosity v and constant density ρ. The dimensionless governing equations written in Cartesian coordinates ($i, j, k = 1, 2, 3$) are given by:

$$\frac{\partial u_i}{\partial x_i} = 0 \tag{1}$$

$$\frac{\partial u_i}{\partial t} + \frac{\partial (u_j u_i)}{\partial x_j} = -\frac{\partial p}{\partial x_i} + \frac{1}{Re}\frac{\partial^2 u_i}{\partial x_j \partial x_j} \tag{2}$$

The dimensionless quantities $x_i = (x, y, z)$, $u_i = (u, v, w)$, p and t denote the coordinate space, velocity component in the x_i direction, hydrodynamic pressure and time, respectively. The scales used for the dimensionalization are H, v/H, $\rho v^2/H^2$, and H^2/v respectively. The Reynolds number Re is based on the cavity length H and the lid velocity u_0 as: $Re = u_0 H/v$.

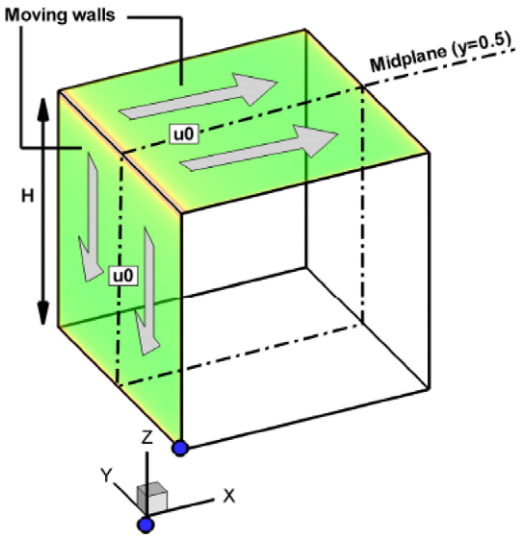

Fig. 1. The geometric model of the two sided non-facing lid driven cubical cavity.
Fig. 1. Modèle géométrique de la cavité cubique doublement entrainée en des faces adjacentes.

Velocity boundary conditions (see Fig. 1) take the following form:

At $z = 1$: (moving wall) $u = 1$, $v = 0$, and $w = 0$,
At $x = 0$: (moving wall) $u = v = 0$, and $w = -1$,
At $x = 1$, $y = 0$, $y = 1$, and $z = 0$: $u = v = w = 0$.

3. Numerical method

Because we are interested in the transition to unsteadiness in which the time accuracy is of great importance, we have chosen to use a second order stepping scheme. This second order scheme is based upon two main ingredients:

(i) The time derivative in the momentum equations is approximated by a second order Euler backward scheme:

$$\left(\frac{\partial f}{\partial t}\right)^{n+1} = \frac{3f^{n+1} - 4f^n + f^{n-1}}{2\Delta t} + \sigma\left(\Delta t^2\right)$$

where $f = u$, v or w.

(ii) The linear terms are evaluated at time $(n+1)\Delta t$ whereas the non-linear part N is explicitly evaluated at time $(n+1)\Delta t$ by means of an Adams–Bashforth extrapolation:

$$N^{n+1} = 2N^n - N^{n-1}.$$

The velocity-pressure coupling present in the continuity and the momentum equations is handled by using the projection method [14]. At each time, the momentum equations for a provisional velocity field that may not be divergence free, are solved. A Poisson equation with homogeneous boundary conditions is then solved and leads to update pressure and free divergence velocity fields. A finite volume method [15] on a staggered grid system is employed to discretize the system of equations to be solved. The QUICK scheme of Hayase et al. [16] is employed to minimize the numerical diffusion for the advective terms.

The discretized equations are solved using the red and black point successive over-relaxation method with optimum relaxation factors, except the Poisson equation which is solved using an accelerated full multigrid method (FMG) [17]. Results provide the superiority of the FMG multigrid method against single grid calculations using the so-called V-cycle and optimal relaxation parameters. The global convergence was guaranteed by controlling the L_2-residuals norm of all equations to be solved by setting its variation to less then 10^{-7}.

4. Results and discussion

The 3D-TSNFL cubical cavity is examined. Firstly, computations were performed at low Reynolds numbers from $Re = 100$ and steady solutions was established. The fluid is taken initially at rest.

The steady state was considered as achieved according to the following criterion:

$$\underbrace{\max}_{ijk}\left(\left|\frac{u_{ijk}^{n+1}-u_{ijk}^{n}}{u_{ijk}^{n}}\right|,\left|\frac{v_{ijk}^{n+1}-v_{ijk}^{n}}{v_{ijk}^{n}}\right|,\left|\frac{w_{ijk}^{n+1}-w_{ijk}^{n}}{w_{ijk}^{n}}\right|\right)\leqslant 10^{-4}$$

where the superscript n denotes the iteration time levels, and (i, j, k) refers to the index nodes. This condition requires a dimensionless final time of about 600.

Because of the presence of large gradients near the walls, we generate a centro-symmetric grid with clustering near the walls using following grid point distribution:

$$x_i = \frac{1}{2}\left(1+\frac{\tanh[\gamma(2i/N-1)]}{\tanh(\gamma)}\right)$$

where $\gamma = 1.25$ and $1 \leqslant i \leqslant N$. Similar grid point distribution has been used in the three directions of the cavity.

Accurate numerical solutions for the three-dimensional lid-driven cavity flows at $Re = 1000$, using spectral methods has been performed by Albensoeder and Kuhlmann [2], and our intention here is to compare our solutions with theirs. A systematic grid refinement test has been done using non-uniform staggered grids of 32^3, 48^3 and 64^3 at $Re = 1000$. The extrema of the u-, v- and w-velocity components as well as their locations have been reported in Table 1. Plots of the u- and w-velocity components along the vertical and horizontal centerlines on the symmetry plane are shown in Fig. 2, together with the results from the pseudo-spectral calculations of [2]. It can be seen from Table 1 and Fig. 2 that the results from our 3D-code agree reasonably well with whose of [2], and deviation from Albensoeder et al.'s results is about 1%. Our results seem to be better than those of Refs. [5] and [6].

It also can be concluded from Table 1 that a grid of 64^3 nodes with clustering towards the cavity walls produces grid independent solution. Thus, all the computations are carried out using a 64^3 grid size with a time step of 0.01.

The 3D flow structure in a one sided lid driven cavity [2–4] presents a large primary eddy which occupies the core of the flow and two secondary eddies at the vertical central plane. We do not show them here, instead we plot in Fig. 3 isosurfaces of absolute velocity $|\vec{v}| = \sqrt{u^2+v^2+w^2} = 0.15$ at Reynolds number $Re = 1000$. It can be seen, that only the speed core of the fluid is high. Hence energy is transferred from the top moving wall to the core of the cavity and regains the top wall by accelerated motion.

The steady flow structure obtained numerically for the 3D-TSNFL at $Re = 500$ is analyzed in the following. As initial conditions for the simulations, the fluid is considered at rest. Fig. 4 shows the stream traces at the mid-plane ($y = 0.5$) of the 3D-TSNFL cavity flow at $Re = 500$. Two primary and two secondary vortices are formed with a perfectly symmetric patterns about the diagonal cavity. Thus, the 3D-TSNFL flow structure exhibits the same qualitative eddy structures as its 2-D counterpart about the central plane. This figure agrees qualitatively with the pictures presented by Wahba [9] according to the 2D-case. We also performed simulations according to the 2D-TSNFL cavity flow

Table 1
Grid independence at $Re = 1000$ for the lid-driven cubical cavity and comparison of our results with those of Albensoeder et al. [2], Lo et al. [5], and Ding et al. [6].

Tableau 1
Indépendance de la grille à $Re = 1000$ pour la cavité cubique entrainée et comparaison de nos résultats avec ceux de Albensoeder et al. [2], Lo et al. [5], et Ding et al. [6].

Ref. Grid	$u_{\min}$	$z_{\min}$	$w_{\min}$	$x_{\min}$	$w_{\max}$	$x_{\max}$
Present work 32^3	−0.2670297	0.1287	−0.4133509	0.9214	0.2351729	0.1023
Present work 48^3	−0.2744732	0.1239	−0.4294606	0.9100	0.2416644	0.1063
Present work 64^3	−0.2769995	0.1227	−0.4295692	0.9041	0.2438928	0.1084
	(1.2%)	(1.2%)	(1.25%)	(0.6%)	(1.11%)	(0.6%)
Ref. [2] $96 \times 96 \times 64$	−0.2803833	0.12419	−0.4350186	0.90957	0.2466511	0.10913
Ref. [5] 101^3	−0.26714	0.12	−0.41534	0.92	0.23647	0.12
Ref. [6] 49^3	−0.258	0.12	−0.414	0.92	0.225	0.12

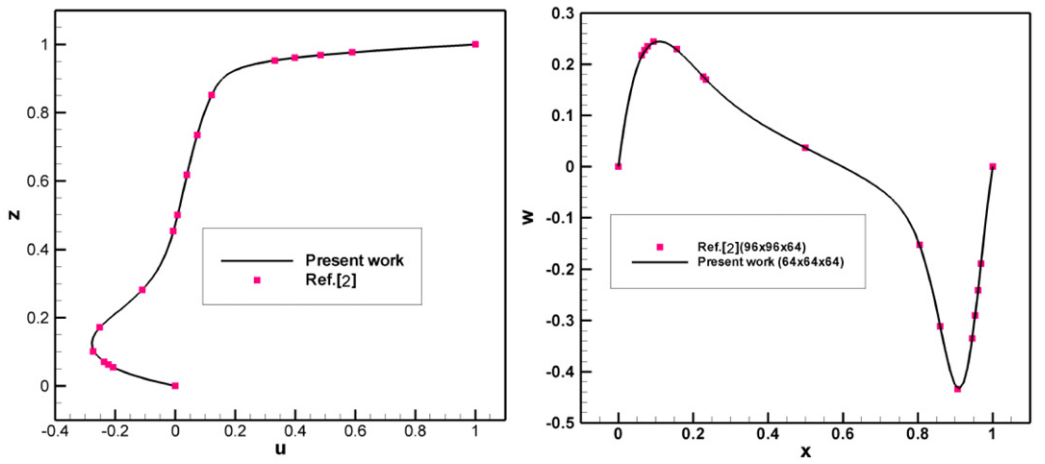

Fig. 2. Velocity profiles along centerlines of the lid-driven cubical cavity at Reynolds number ($Re = 1000$) compared with those of Ref. [2].

Fig. 2. Profiles de vitesse à la ligne centrale de la cavité cubique entrainée comparés à ceux de la référence [2].

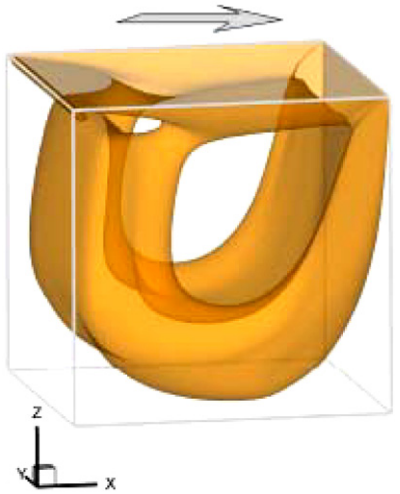

Fig. 3. Isosurface of magnitude of velocity $|\vec{v}| = 0.15$ of the lid-driven cubical cavity at Reynolds number ($Re = 1000$).

Fig. 3. Iso surfaces du module de la vitesse $|\vec{v}| = 0.15$ en cavité cubique entrainée et à un nombre de Reynolds ($Re = 1000$).

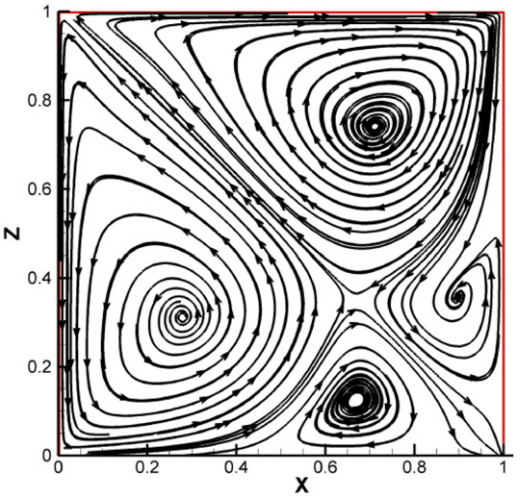

Fig. 4. Stream traces at the mid-plane ($y = 0.5$) of the 3D-TSNFL cavity flow at Reynolds number ($Re = 500$).

Fig. 4. Trajectoires de particule au plan médian ($y = 0.5$) de la cavité doublement entrainée à un nombre de Reynolds ($Re = 500$).

on a non-uniform 256^2 grid (results were submitted in the present revue). It has been observed that the 3D-TSNFL almost reproduces the 2D-TSNFL at the mid-plane $y = 0.5$ for $Re = 500$.

The u- and w-contours are shown in Fig. 5(a), (b) in the horizontal and vertical mid-planes of the cavity. For each component, three rolls are observed in the x–z plane: a central large clockwise/anticlockwise roll and two asymmetric clockwise/anticlockwise rolls close to the walls.

Fig. 6 presents iso surfaces of $|\vec{v}| = 0.15$ and reveals similar behavior of the topology flow seen in Fig. 4. The steady 3D-TSNFL flow obtained at $Re = 500$ is also shown in Fig. 7 in terms of both isosurfaces and isocontours of the velocity gradient tensor component. A high velocity gradient is observed in the spanwise direction close to the two primary vortices.

Since the 3D-TSNFL flow has never been computed previously, we shall provide benchmark data for $Re = 500$. We report in Table 2 our benchmark solutions obtained with our finite volume multigrid code. The table summarizes the u- and w-components at the mid-plane $y = 0.5$ versus z and x coordinates respectively. The corresponding plot

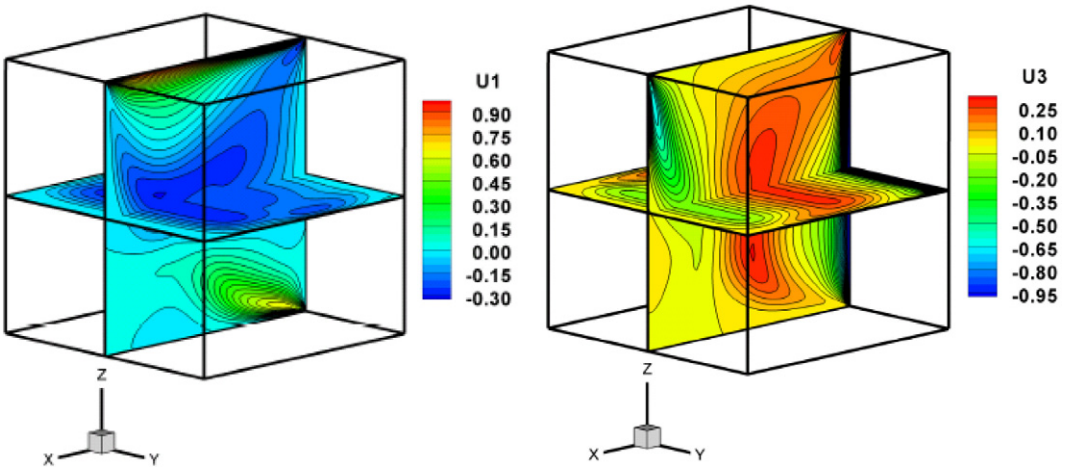

Fig. 5. Velocity component contours of (a) u and (b) w at $Re = 500$.

Fig. 5. Iso-contours des composantes de la (a) u (b) w à $Re = 500$.

Table 2
Benchmark solutions on the 3D-TSNFL cavity flow at $Re = 500$.

Tableau 2
Solutions benchmark de l'écoulement 3D-TSNFL à un nombre de Reynolds $Re = 500$.

x or z	u	w	x or z	u	w
0.00000000	0.00000000	−1.00000000	0.51150640	−0.24202710	0.22246850
0.00333708	−0.00094761	−0.95094250	0.53448410	−0.25677480	0.19982570
0.01023669	−0.00116989	−0.84643550	0.55735710	−0.26450030	0.17500610
0.01759887	0.00045987	−0.73668400	0.58005720	−0.26383170	0.14781820
0.02544694	0.00417619	−0.62673680	0.60251790	−0.25467630	0.11782950
0.03380427	0.01019511	−0.52180040	0.62467590	−0.23811580	0.08507096
0.04269404	0.01869448	−0.42650420	0.64647110	−0.21593530	0.05016490
0.05213903	0.02978594	−0.34418050	0.66784780	−0.19009710	0.01409022
0.06216134	0.04347661	−0.27635530	0.68875470	−0.16235560	−0.02204059
0.07278213	0.05962002	−0.22263380	0.70914570	−0.13406520	−0.05707803
0.08402129	0.07785931	−0.18104040	0.72897970	−0.10614600	−0.08982712
0.09589712	0.09757143	−0.14869430	0.74822150	−0.07914296	−0.11906060
0.10842590	0.11782870	−0.12256420	0.76684110	−0.05331957	−0.14356270
0.12162170	0.13740020	−0.10004470	0.78481440	−0.02875045	−0.16222750
0.13549560	0.15481690	−0.07922164	0.80212240	−0.00539329	−0.17420630
0.15005570	0.16851030	−0.05885839	0.81875170	0.01686394	−0.17906680
0.16530640	0.17701110	−0.03822671	0.83469360	0.03818667	−0.17691270
0.18124830	0.17916390	−0.01691143	0.84994430	0.05882512	−0.16841310
0.19787760	0.17429990	0.00533776	0.86450440	0.07919434	−0.15472340
0.21518560	0.16231640	0.02868646	0.87837830	0.10002250	−0.13731270
0.23315890	0.14364620	0.05324699	0.89157410	0.12254620	−0.11774900
0.25177850	0.11913900	0.07906218	0.90410290	0.14867950	−0.09750067
0.27102030	0.08990133	0.10605820	0.91597870	0.18102820	−0.07779796
0.29085430	0.05714921	0.13397270	0.92721790	0.22262380	−0.05956808
0.31124530	0.02210986	0.16226230	0.93783870	0.27634780	−0.04343366
0.33215220	−0.01402209	0.19000850	0.94786100	0.34417570	−0.02975133
0.35352890	−0.05009776	0.21585870	0.95730600	0.42650250	−0.01866743
0.37532410	−0.08500518	0.23805920	0.96619570	0.52180150	−0.01017477
0.39748210	−0.11776540	0.25464740	0.97455310	0.62674010	−0.00416171
0.41994280	−0.14775460	0.26383550	0.98240110	0.73668830	−0.00045046
0.44264290	−0.17493970	0.26453660	0.98976330	0.84643940	0.00117500
0.46551590	−0.19975310	0.25683700	0.99666290	0.95094430	0.00094914
0.48849360	−0.22239020	0.24210350	1.00000000	1.00000000	0.00000000

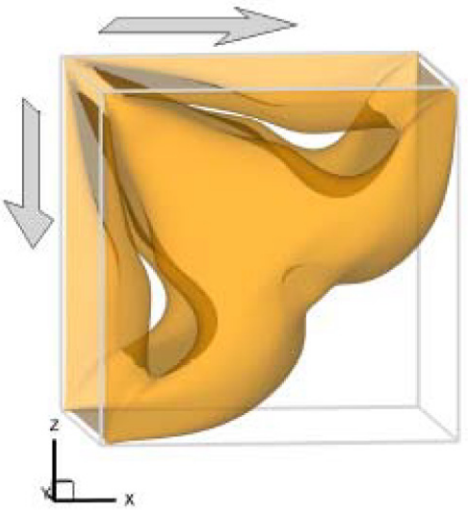

Fig. 6. Isosurface of magnitude of velocity $|\vec{v}| = 0.15$ of the 3D-TSNFL cavity at Reynolds number ($Re = 500$).

Fig. 6. Iso surfaces du module de la vitesse $|\vec{v}| = 0,15$, en cavité 3D-TSNFL à un nombre de Reynolds ($Re = 500$).

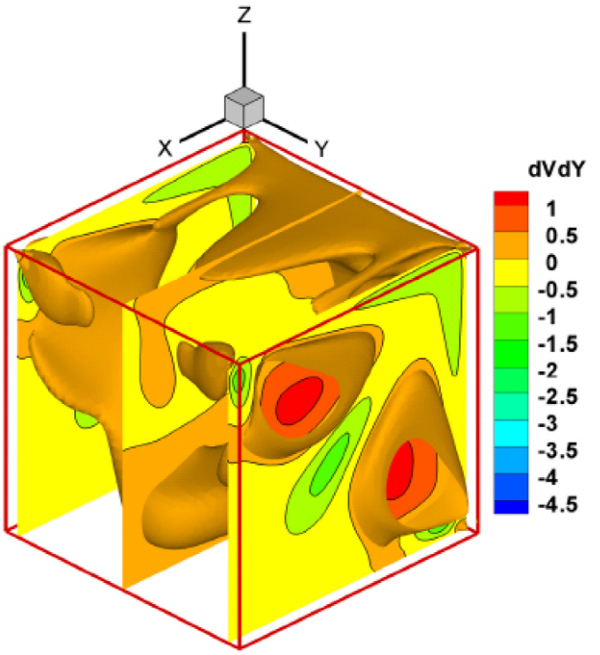

Fig. 7. Iso contours and iso surfaces of the tensor gradient velocity component (dV dy).

Fig. 7. Iso contours et iso surfaces de la composante du tenseur de gradient de vitesse (dV dy).

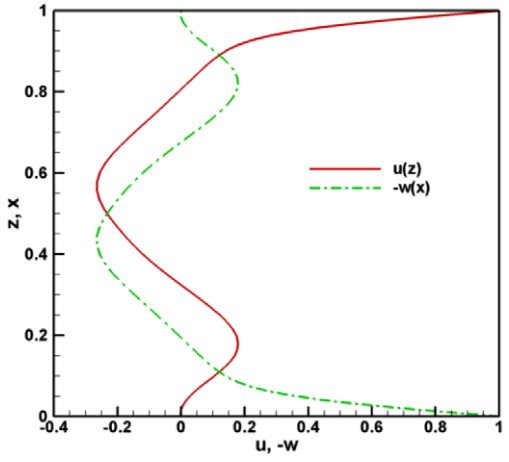

Fig. 8. u- and w-velocity components at the centerline $y = 0.5$ for $Re = 500$.

Fig. 8. Composantes de vitesse u et w au plan médian $y = 0,5$ et $Re = 500$.

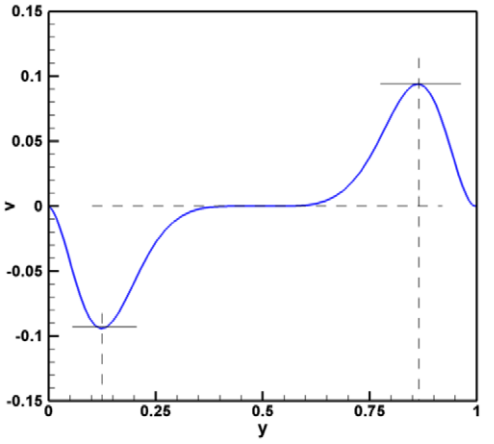

Fig. 9. Spanwise velocity component v (0.5, y, 0.5).

Fig. 9. Composante de vitesse transverse v (0,5, y, 0,5).

(Fig. 8) shows a perfectly symmetry about the cavity center. The transverse v-component is depicted in Fig. 9. One can clearly see that the v-velocity component reduces to near zero in the enclosure central region (between $x = 0.35$ and $x = 0.65$) and the fluid flow is confined adjacent to the end walls.

Calculations were performed for several Reynolds numbers from $Re = 500$ to 700, taking as initial conditions the converged solution obtained at $Re = 500$. With the increase of Re beyond a certain critical value the 3D-TSNFL flow becomes unstable and bifurcates. Representatives profiles at the position $x = 0.25$, $y = 0.5$ and 0.25 of the cavity, for

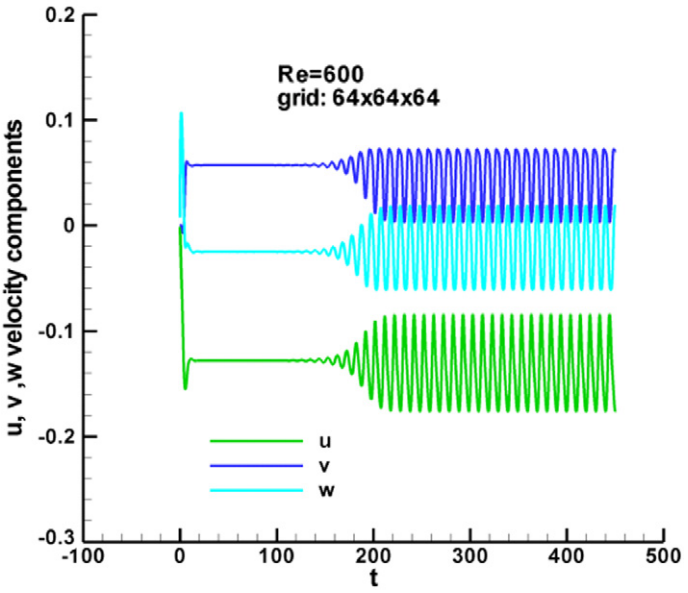

Fig. 10. Periodic behavior of the 3D-TSNFL flow at $Re = 600$ of the u, v, w-components at the monitoring point A $(0.25, 0.5, 0.25)$.

Fig. 10. Comportement périodique de l'écoulement tridimensionnel, composantes u, v et w, de la cavité doublement entrainée à $Re = 600$ au point de contrôle A $(0{,}25, 0{,}5, 0{,}25)$.

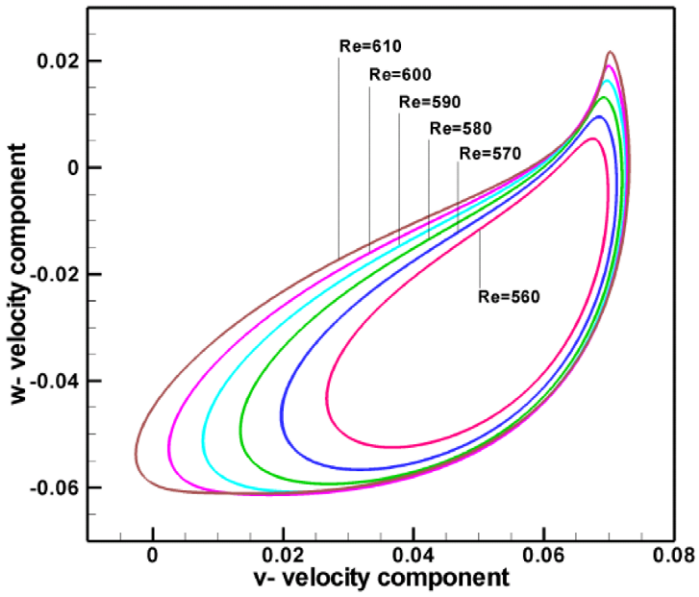

Fig. 11. Phase diagrams (v, w) for different Re numbers at the mid-plane $y = 0.5$.

Fig. 11. Diagrammes de phase (v, w) à différents nombres de Re au plan médian $y = 0{,}5$.

u-, v-, and w-velocity component velocity for various Re number were obtained but not presented here. An example to illustrate the time-dependent solution of the 3D-TSNFL flow is shown in Fig. 10. It can be seen that all the velocity components are periodic with the same period. The frequency of oscillation was found to be 0.101.

The Re has been increased in step of 10. To verify the periodic behavior of the flow, a phase plot of v-velocity against w-velocity at the above located point for different Re is shown in Fig. 11.

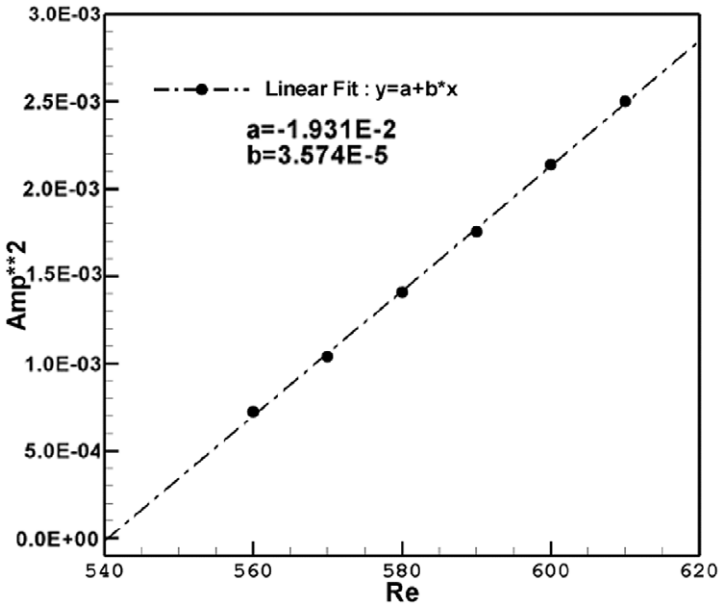

Fig. 12. Square of the u-velocity component magnitude fluctuation versus the Reynolds number.

Fig. 12. Carré de la fluctuation de l'amplitude de la composante u de la vitesse en fonction du nombre de Reynold.

It is known for the Hopf bifurcation [18,19] that the amplitude of the solution grows with the square-root of the bifurcation parameter. This means that the square of the u-velocity fluctuation amplitude Amp^2 should be proportional to the difference of the Re and the critical Re_c number after the bifurcation has taken place. It should be noted that the u-velocity fluctuation amplitude Amp is defined as: $Amp = |u_1 \max(A,t) - u_1 \min(A,t)|/2$, where A is the monitoring point of coordinates $(0.25, 0.5, 0.25)$. Thus, we plot in Fig. 12 Amp^2 as a function of Re, where the symbols and the solid lines denote our numerical data and the lines of best fit, respectively. This line can be extrapolated to where it crosses the zero axis to approximate the bifurcation point, which gives a critical value of approximately $Re_c = 540 \pm 2\%$.

5. Conclusion

Simulations of the 3D-TSNFL cavity flow have been performed for various Reynolds numbers. Multigrid is used as convergence accelerator to provide solutions on a non-uniform staggered grid of 64^3 grid nodes. According to the steady regime, it is found that the 2D-TSNFL approximation can present the flow in the vertical mid-plane of the 3D-TSNFL cavity. The numerical experiments reveal that the first Hopf bifurcation takes place at $Re_c = 540 \pm 2\%$, and a periodic solution is described at $Re = 600$ with a frequency of about 0.101 dimensionless time. Furthermore, the transition of flow occurs earlier, at lower Re, for the 3D-TSNFL relative to the 2D-LDC flow.

References

[1] P.N. Shankar, M.D. Despande, Annu. Rev. Fluid Mech. 32 (2000) 93–136.
[2] S. Albensoeder, H.C. Kuhlmann, Accurate three-dimensional lid-driven cavity flow, J. Comput. Phys. 206 (2005) 536–558.
[3] O. Botella, R. Peyret, Benchmark spectral results on the lid-driven cavity flow, Comput. & Fluids 27 (1998) 421–433.
[4] C.-H. Bruneau, M. Saad, The 2D lid-driven cavity problem, Comput. & Fluids 35 (2006) 326–348.
[5] D.C. Lo, K. Murugesan, D.L. Young, Numerical solution of three-dimensional velocity–vorticity Navier–Stokes equations by finite difference method, Int. J. Numer. Meth. Fluids (2004).
[6] H. Ding, C. Shu, K.S. Yeo, D. Xu, Numerical computation of three-dimensional incompressible viscous flows in the primitive variable form by local multiquadric differential quadrature method, Comput. Methods Appl. Mech. Engrg. 195 (2006) 516–533.
[7] H.C. Kuhlmann, M. Wanschura, H.J. Rath, Flow in two-sided lid-driven cavities: non-uniqueness, instability, and cellular structures, J. Fluid Mech. 336 (1997) 267–299.

[8] W.-J. Luo, R.-J. Yang, Multiple fluid flow and heat transfer solutions in a two-sided lid-driven cavity, Int. J. Heat Mass Transfer 50 (2007) 2394–2405.
[9] E.M. Wahba, Multiplicity of states for two-sided and four-sided lid driven cavity flows, Computers & Fluids (2008), doi:10.1016/j.compfluid.2008.02.001.
[10] F. Auteri, N. Parolini, L. Quartapelle, Numerical investigation on the stability of singular driven cavity flow, J. Comput. Phys. 183 (2002) 1–25.
[11] Min Chan Kim, Sin Kim, Chang Kyun Choi, The convective stability of circular Couette flow induced by a linearly accelerated inner cylinder, Eur. J. Mech. B/Fluids 25 (2006) 74–82.
[12] J.R. Koseff, R.L. Street, Visualization studies of a shear driven three-dimensional recirculating flow, ASME J. Fluid Eng. 33 (1984) 594–602.
[13] J. Chicheportiche, X. Merle, X. Gloerfelt, J.-C. Robinet, Direct numerical simulation and global stability analysis of three-dimensional instabilities in a lid-driven cavity, C. R. Mecanique 336 (2008).
[14] D.L. Brown, R. Cortez, M.L. Minion, Accurate projection methods for the incompressible Navier–Stokes equations, J. Comput. Phys. 168 (2001) 464–499.
[15] S.V. Patankar, A calculation procedure for two-dimensional elliptic situations, Numer. Heat Transfer 34 (1981) 409–425.
[16] T. Hayase, J.A.C. Humphrey, R. Greif, A consistently formulated QUICK scheme for fast and stable convergence using finite-volume iterative calculation procedures, J. Comput. Phys. 98 (1992) 108–118.
[17] N.B. Cheikh, B.B. Beya, T. Lili, Benchmark solution for time-dependent natural convection flows with an accelerated full-multigrid method, Numer. Heat Transfer B 52 (2007) 131–151.
[18] H. Wang, S. Xin, P. Le Quéré, Etude numérique du couplage de la convection naturelle ave le rayonnement de surfaces en cavités remplie d'air, C. R. Mecanique 334 (2006) 48–57.
[19] J. Shen, Hopf bifurcation of the unsteady regularized driven cavity flow, J. Comput. Phys. 95 (1991) 228–245.